JVST A
Journal of Vacuum Science & Technology A

Using the inelastic background in hard x-ray photoelectron spectroscopy for a depth-resolved analysis of the CdS/Cu(In,Ga)Se_2 interface

Cite as: J. Vac. Sci. Technol. A **39**, 063216 (2021); https://doi.org/10.1116/6.0001336
Submitted: 05 August 2021 • Accepted: 29 September 2021 • Published Online: 25 October 2021

Dirk Hauschild, Ralph Steininger, Dimitrios Hariskos, et al.

JVST A
Journal of Vacuum Science & Technology A

ARTICLE

avs.scitation.org/journal/jva

Using the inelastic background in hard x-ray photoelectron spectroscopy for a depth-resolved analysis of the CdS/Cu(In,Ga)Se_2 interface

Cite as: J. Vac. Sci. Technol. A 39, 063216 (2021); doi: 10.1116/6.0001336
Submitted: 5 August 2021 · Accepted: 29 September 2021 ·
Published Online: 25 October 2021

Dirk Hauschild,[1,2,3,a)] Ralph Steininger,[1] Dimitrios Hariskos,[4] Wolfram Witte,[4] Sven Tougaard,[5] Clemens Heske,[1,2,3] and Lothar Weinhardt[1,2,3,b)]

AFFILIATIONS

[1]Institute for Photon Science and Synchrotron Radiation (IPS), Karlsruhe Institute of Technology (KIT), Eggenstein-Leopoldshafen 76344, Germany
[2]Institute for Chemical Technology and Polymer Chemistry (ITCP), Karlsruhe Institute of Technology (KIT), Karlsruhe 76131, Germany
[3]Department of Chemistry and Biochemistry, University of Nevada, Las Vegas (UNLV), Las Vegas, Nevada 89154
[4]Zentrum für Sonnenenergie-und Wasserstoff-Forschung Baden-Württemberg (ZSW), Meitnerstraße 1, 70563 Stuttgart, Germany
[5]Department of Physics, Chemistry and Pharmacy, University of Southern Denmark, DK-5230 Odense M, Denmark

Note: This paper is a part of the Special Collection Commemorating the Career of Charles S. Fadley.

[a)]Author to whom correspondence should be addressed: dirk.hauschild@kit.edu
[b)]Electronic mail: lothar.weinhardt@kit.edu

ABSTRACT

The inelastic background of hard x-ray photoelectron spectroscopy data is analyzed to paint a depth-resolved picture of the CdS/Cu(In,Ga)Se_2 (CdS/CIGSe) layer structure. The CdS/CIGSe interface is the central component in next-generation chalcopyrite thin-film photovoltaic devices. By analyzing both, the (unscattered) core-level peaks and the inelastic background, and by varying the excitation photon energy from 2.1 up to 14 keV, we can derive photoemission information over a broad range of electron kinetic energies and, hence, sampling depths. With this complementary information, the CdS film thickness of a CdS/CIGSe interface can be accurately determined as a function of the CdS deposition time. For the thinner CdS films, the film thickness can be shown to vary laterally. Furthermore, small amounts of Se and process-related Rb can be detected in a thin (~2 nm) surface layer of all investigated CdS films.

I. INTRODUCTION

Surfaces and interfaces play a crucial role for the function and performance of electronic devices such as batteries, solar cells, and catalysts. The electronic and chemical properties at these surfaces and interfaces often differ significantly from the bulk properties of the involved materials, which is particularly true for "real-world" (i.e., nonideal) systems, for which compositional gradients, diffusion, and intermixing play important roles.[1–4] For an insight-driven optimization of such devices, a detailed characterization of these effects is necessary. This requires characterization techniques with suitable information depth that can probe the volume of interest, ideally in a depth-resolved fashion. Most commonly, destructive techniques like secondary ion mass spectroscopy,[5,6] x-ray photoelectron spectroscopy (XPS) in a depth-profiling mode,[7,8] or glow discharge optical emission spectroscopy[9,10] are employed that combine the removal of material from the surface region with a surface-sensitive and/or element-specific probe to give a depth-resolved picture of the chemical composition. However, these techniques are well known to suffer from, e.g.,

surface and matrix effects, preferential sputtering, implantation, amorphization, crater formation and many other effects, making a correct interpretation of the data extremely challenging and the information content of these methods highly questionable.[5,9,11,12]

Such effects can be avoided by using nondestructive and chemically sensitive characterization techniques like XPS, x-ray emission spectroscopy (XES), or x-ray absorption spectroscopy (XAS). The challenge with these techniques is to vary their surface sensitivity to gain depth information. This requires varying the characteristic attenuation length λ or the path length d that govern the exponential decay $I = I_0 \cdot e^{-d/\lambda}$ of the (unscattered) signal of these techniques. Great success has been achieved by using a combination of techniques with significantly different λ, e.g., XPS and XES,[1,13–16] or by employing different yield modes in XAS,[17] but suitable absorption edges and emission transitions are required. The "effective" attenuation length λ can also be varied using angle-dependent measurements[18,19] but this approach only works well for flat surfaces, which are usually not found in real-world systems when cost-efficiency is required.

For XPS, the electron inelastic mean free path (IMFP) λ is a function of the kinetic energy, which can be employed either by comparing different peaks of the same element at different kinetic energies or by varying the kinetic energy of a given XPS line by using different photon excitation energies. In recent years and with much pioneering impetus by Chuck Fadley and co-workers,[20–23] the range of accessible kinetic energies was extended by the development of new synchrotron beamlines optimized for hard x-ray photoelectron spectroscopy (HAXPES). With these new setups, λ can be increased significantly (e.g., from ∼3 nm for laboratory-based XPS up to ∼16 nm for HAXPES with photon energies of 15 keV).[24–26] Thanks to Chuck's energetic leadership, HAXPES is now a powerful technique to study deeper layers of samples with complex inner structures.[27–29]

In most cases, the intensity and attenuation of the *unscattered* (or elastically scattered) photoelectron peaks ("main lines") are analyzed to derive information about the depth distribution of the respective element. While such an analysis already gives valuable insights, the information content can be drastically increased by also analyzing the shape of the inelastic background, i.e., the overall spectral structure formed by the *inelastically* scattered electrons. This background contains information on the elemental distribution[30,31] for depths of up to 10 or even 20 λ,[32–34] a length scale on which the main line is not visible at all. Since the average electron energy loss is roughly proportional to the distance the electron has traveled in the material,[30,35] the kinetic-energy axis is also an "energy-loss" axis and can even loosely be considered as a kind of "depth-information" axis. To do this, a few 100 eV of inelastic background has to be measured at the low-kinetic-energy side of the peak. This works particularly well for HAXPES, for which λ is large and only a few Auger transitions[36–40] are present at higher kinetic energies. The background can, therefore, often be measured over a wide energy range without interfering signals from other elements. The potential of this approach has been extensively explored with "conventional" XPS for more than 30 years[30–32] and in recent years also with HAXPES. The accuracy for the application with HAXPES has mainly been evaluated by the analysis of model systems[31,33,34,41,42] but also first steps to address applied materials have been taken.[43]

In this paper, we present a model study of the inelastic background in HAXPES data together with the corresponding photoemission main lines to draw a depth-resolved picture of the $CdS/Cu(In,Ga)Se_2$ (CdS/CIGSe) interface. This heterojunction is the central component in chalcopyrite thin-film solar cells, and very high power conversion efficiencies (up to ∼23%) can be achieved.[44–46] This is particularly true if the CIGSe absorber is exposed to a heavy-alkali postdeposition treatment (PDT),[45,46] which significantly modifies the chemical structure at the surface/interface. In earlier studies, we have shown that a RbF-PDT leads to a favorable conduction band alignment,[47] an improved CdS growth with chemical bath deposition (CBD),[48] and diffusion of rubidium and sodium toward the surface of the CdS layer.[13] Other studies also showed improved CIGSe bulk properties after PDT.[49–51] Earlier XPS/XES studies of CdS/CIGSe and similar interfaces have furthermore shown a S-Se intermixing at the interface, indicating the (further) complexity of this real-world heterojunction.[15,52,53] With the present HAXPES study, using excitation photon energies from 2.1 up to 14 keV (as provided by the newly built X-SPEC beamline,[54] see below), we can further refine this complex picture of the CBD-CdS/RbF-PDT CIGSe interface by analyzing the photoelectron main lines *and the inelastic background signals*.

II. EXPERIMENT

$CdS/Cu(In,Ga)Se_2$ heterojunctions were prepared at the Zentrum für Sonnenenergie-und Wasserstoffforschung Baden Württemberg. The CIGSe solar cell absorbers were grown in an in-line multistage process by coevaporating Cu, Ga, In, and Se onto a sputtered Mo/soda-lime glass substrate at elevated temperatures.[55] After completion of the CIGSe layer formation, the absorbers were exposed *in situ* to an RbF postdeposition treatment under selenium atmosphere (PDT).[46] The Ga/(Ga + In) ratio of the absorber bulk was ∼0.33, as determined by x-ray fluorescence spectroscopy. Subsequently, the absorbers were rinsed in an 1.5 M ammonia solution in order to remove excess RbF material. Afterward, CdS buffer layers were deposited onto the CIGSe absorbers by CBD, generating a CdS sample series with increasing thicknesses corresponding to CBD times of 1.5, 3.5, 5.0, 6.5, and 8.5 min. The deposition of the CdS layers were performed at 65 °C from a 200 ml solution containing 1.4 mM $CdSO_4$, 1.5 M NH_4OH, and 0.12 M thiourea. The thickness of the 8.5 min CdS film is estimated as 50 (±5) nm by the interference color of CdS on a molybdenum-coated soda-lime glass substrate, which was grown in the same bath used for the corresponding CIGS sample. Twin CdS/CIGSe samples with a CdS thickness of 50 (±5) nm were further processed to full solar cells (total area of 0.5 cm^2) with an i-ZnO/Al-doped ZnO front contact and achieved average conversion efficiencies of ∼17% without antireflective coating. All samples for the HAXPES surface analysis were briefly exposed to air after growth, sealed under nitrogen atmosphere, and transferred to the Karlsruhe Institute of Technology (KIT), where the samples were unpacked and mounted on a sample holder in an Ar-filled glovebox. The samples were then transferred to the ultrahigh vacuum chamber of the experimental station. The total air exposure time of each sample was less than 5 min.

HAXPES measurements were performed at the X-SPEC double-undulator beamline[54] of the KIT Synchrotron (KARA

accelerator) using a Phoibos 225 electron energy analyzer (SPECS). X-SPEC is a novel and unique undulator-based spectroscopy beamline, enabling experiments with excitation energies from 70 eV to 15 keV. For the present data set, experiments were conducted with photon energies of ~2.1, 6.3, 9.0, 12, and 14 keV using the Si(111) reflection of the Double Crystal Monochromator of the X-SPEC beamline.

The background analysis of the HAXPES spectra was performed with the software package QUASES-TOUGAARD Ver. 7.50.[26]

III. RESULTS AND DISCUSSION

Selected HAXPES survey spectra of the CIGSe absorber, as well as the 5.0 and 8.5 min CdS/CIGSe samples, are shown in Fig. 1 (measured with an excitation energy of 12 keV). Survey spectra of all samples at other excitation energies are plotted in the supplementary material.[62]

As expected, the CIGSe spectrum shows many absorber-related lines, e.g., Se 2s and 2p, Ga 2p, Cu 2p, and In 3s, 3p, and 3d. For the 5.0 min CdS/CIGSe survey spectrum, strong Cd- and S-related peaks are detected, while the absorber-related peaks are strongly attenuated by the CdS layer. However, we find clear "steps" in the background, extending for several hundred electron volts, at the high-binding/low-kinetic-energy side of the respective peak positions, which is highlighted for the Se 2s and 2p peaks in the inset of Fig. 1. With further increasing CBD time (8.5 min), these steps decrease in intensity and move further away from the corresponding peak but are still visible (this is best seen in Fig. 2). The decrease in peak intensity and the relative increase of the inelastic background are caused by inelastic scattering of electrons from the respective CIGSe absorber core-level lines as they pass through the CdS overlayer; and these electrons will be analyzed in detail in this paper. To do this, we will focus on the "background region" between the S 1s and Cd 3s core-level lines (i.e., 800–2400 eV, as marked by the red-dashed rectangle in Fig. 1), which only contains CIGSe-related signals (i.e., Se 2s and 2p, Ga 2s and 2p, and In 3s).

The corresponding spectral region was measured with five different photon energies between 2.1 and 14 keV. From these spectra, several aspects of the CdS/CIGSe layer structure can be investigated and will be discussed below, each addressed best with a different combination of experimental parameters:

(1) The overall CdS film thickness: Due to the variation in λ, spectra with lower kinetic energies (i.e., excited with lower photon energies) are better suited for the thinner films, while spectra with higher kinetic energies (i.e., higher photon energies) are best used for the thicker films.
(2) Diffusion/segregation of absorber elements: For the kind of diffusion observed in the present case, the lower photon energy data are suited best.
(3) The homogeneity of the CdS film thickness: This is best addressed with the thinner samples in the set and the full range of available excitation energies.

To obtain a first estimate of the overall thickness of the various solution-grown CdS films, we now discuss the data excited with 14 keV photons, a section of which is plotted for all samples in Fig. 2 (black spectra). At this excitation energy, the kinetic energies in the analyzed "background region" are in the range of ~12–13 keV, which gives a λ of ~16 nm, as determined by the free software QUASES-IMFP-TPP2M (Ref. 26) (which is based on Refs. 24 and 25). With increasing CdS buffer layer thickness, the absorber-related peaks are strongly attenuated (note the multiplication factors of up to ×48, at the left ordinate in Fig. 2) while the relative background intensity of the inelastically scattered electrons increases. For the longest CBD time (8.5 min), no Ga main line is visible, while very small Se 2s and 2p signals are still detectable. This suggests that Ga and Se have different depth distributions after the CBD-CdS/CIGSe interface formation and that some Se may be

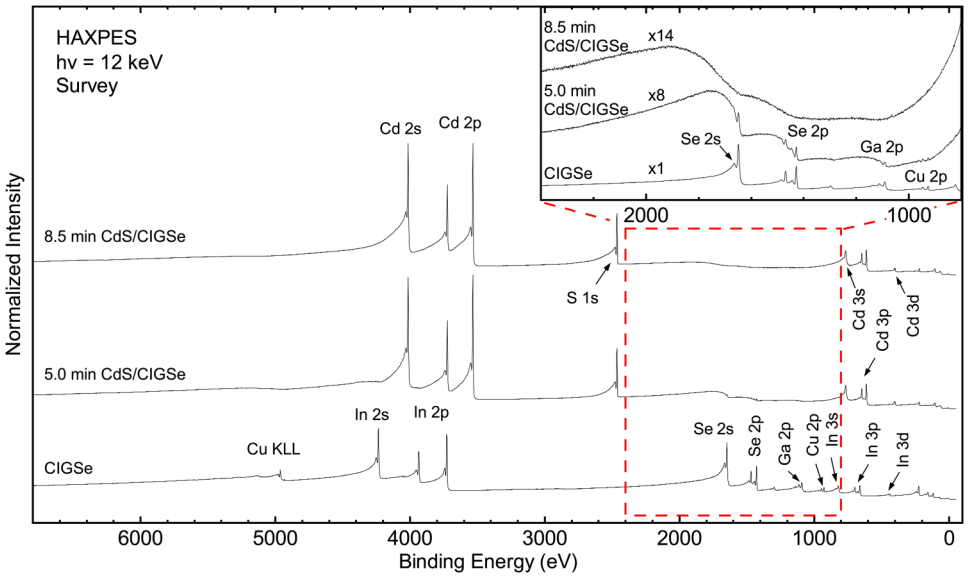

FIG. 1. HAXPES (hν = 12 keV) survey spectra of the CIGSe absorber, the 5.0 min, and the 8.5 min CdS/CIGSe samples (from bottom to top). The inset shows the magnified region marked by the red-dashed rectangle, which contains only CIGSe-related signals (the "background region" for CdS). Prominent photoemission and Auger features are labeled. (Color online.)

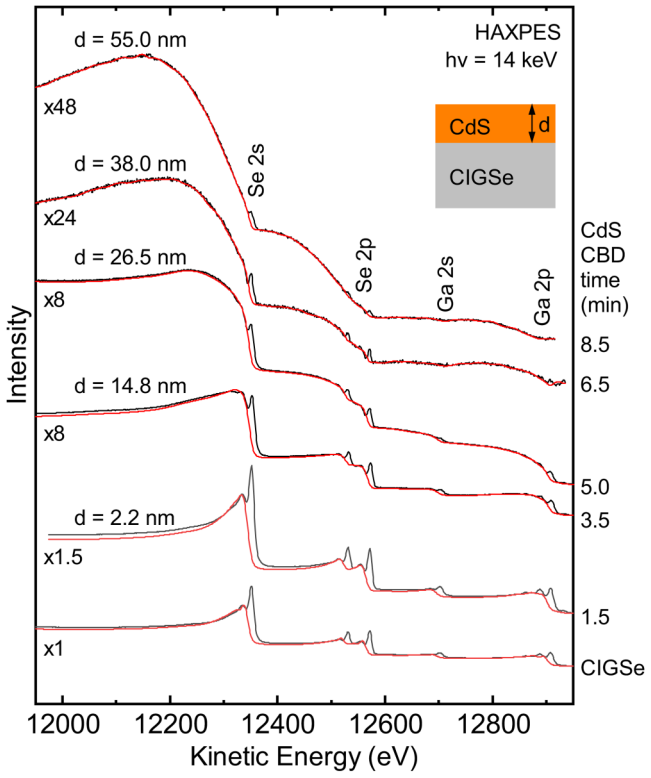

FIG. 2. Se 2s/2p and Ga 2s/2p spectral region for CIGSe and CdS/CIGSe samples with increasing CdS-CBD time, measured with a photon energy of 14 keV. The data are shown in black and the simulated inelastic background (based on the simple model shown in the top right corner) in red. The determined CdS thicknesses as well as the magnification factors are given on the left. (Color online.)

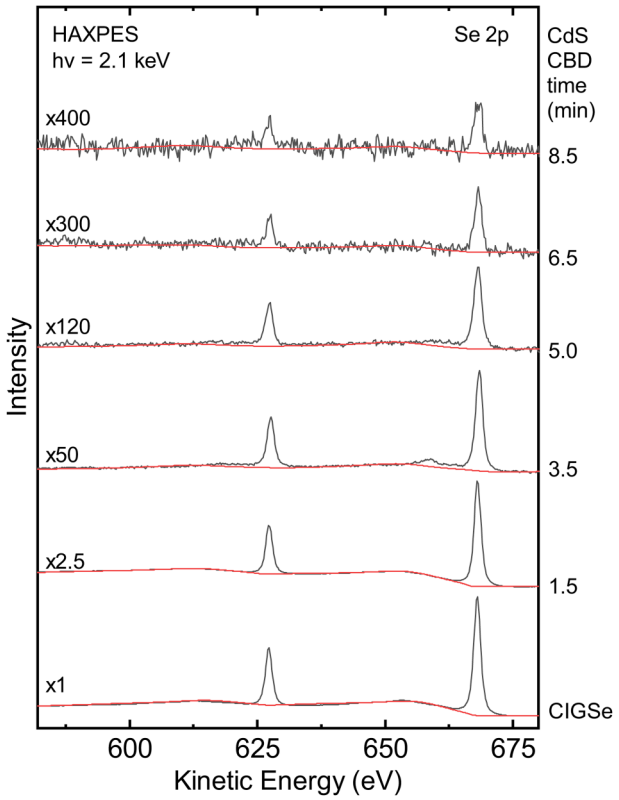

FIG. 3. Se 2p main line and background region for the CIGSe and CdS/CIGSe samples with increasing buffer layer CdS-CBD time, measured at a photon energy of 2.1 keV. Magnification factors are shown on the left. The data are shown in black and the simulated inelastic background in red. (Color online.)

present in the topmost region of the CdS buffer layer. This interpretation is also corroborated by the more surface-sensitive measurements at 2.1 keV excitation energy (where Se 2s and 2p, but no Ga-related signals, are visible for the 8.5 min CdS sample, see further below) as well as by the detailed background analysis in conjunction with Fig. 4.

In addition to the photoemission main lines, distinct variations in the inelastic background at the low-kinetic-energy side of the respective photoelectron peaks are observed. This is best seen for the Se 2s signal at 12 350 eV. In particular, the maximum intensity of the inelastic background shifts to lower kinetic energies with increasing buffer layer thickness, while the onset of the loss-features remains at constant energy. This can be easily understood:[30] for a thicker CdS layer, the majority of the Se 2s photoelectrons faces an increased probability of inelastic scattering events before reaching the surface, and consequently their *average* energy loss increases as well, while the *minimal* possible energy loss remains the same.

To analyze the inelastic background with the QUASES software,[26] we first apply the simplest model in the software, i.e., a CdS layer of homogeneous thickness, on top of the (buried) CIGSe absorber (as sketched at the top right of Fig. 2). We expect this to be a reasonable first approximation since earlier studies indicate that CdS grows quite homogeneously on RbF-PDT treated CIGSe surfaces and that the CdS layer is already closed after 3 min of CBD.[13,48] The CIGSe layer thickness is in the range of 2 μm (Ref. 55) and can, therefore, be set to infinity in the model. For each spectrum, the CdS overlayer thickness in the model was manually adjusted until a good agreement between experiment (black curve) and calculated background (red curve) is achieved. At the same time, the inelastic scattering cross section was optimized in an iterative process such that a good agreement is achieved for *all* CdS thicknesses. The parameters C and D of the inelastic scattering cross-section description[56] $\lambda(E)K(E,T) = \theta(T - T_0) \cdot [(B\,T)/(C - T^2)^2 + DT^2]$ were determined to C = 300 eV^2 and D = 260 eV^2 for CdS and C = 180 eV^2 and D = 80 eV^2 for CIGSe. B was adjusted such that the area under the curve λ(E)K(E,T) is unity. The bandgaps T_0 of the CdS layer and the CIGSe absorber surface were set to 2.4 and 1.4 eV, respectively.[47,57] For the 1.5 and 3.5 min CBD-CdS samples, linear combinations of the CIGSe and CdS inelastic cross sections were used: "0.60 × CIGSe + 0.40 × CdS" for 1.5 min CBD-CdS and "0.09 × CIGSe + 0.91 × CdS" for 3.5 min CBD-CdS.

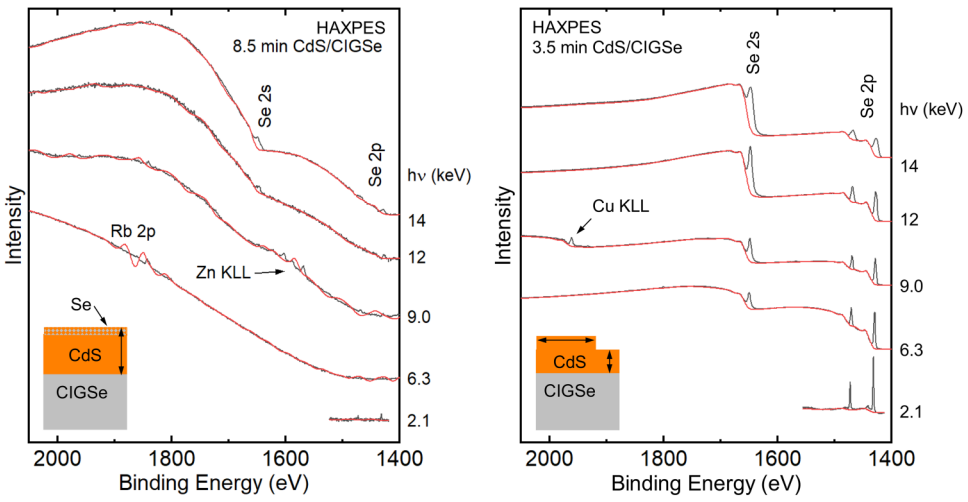

FIG. 4. Se 2s/2p main lines and background regions of the 8.5 min (left) and 3.5 min (right) CdS/CIGSe samples for different photon energies. The data are shown in black and the simulated inelastic background in red. The scheme in the bottom left corner of each panel shows the model used to derive the simulated background. (Color online.)

The resulting background fits and the corresponding CdS thicknesses are shown in Fig. 2. As expected, with increasing CBD time, the determined CdS thickness increases for the analyzed data. The corresponding values are listed in Table I (and summarized in Fig. 5, discussed further below). At 14 keV photon energy, we find a CdS thickness of 55.0 (±5.0) nm for the 8.5 min CBD-CdS layer in agreement with the optically derived nominal thickness estimate of ~50 nm. This is approximately a factor of 3.5 larger than the IMFP of ~16 nm of the measurement. Other CdS samples are best described by a layer thickness that is slightly larger than the estimate—for example, the 14 keV excitation analysis suggests a layer thickness of 26.5 (±3.0) nm for the estimated 18–20 nm sample. Overall, we find a very good description of the background of the thicker buffer layers over the entire energy range but deviations are clearly visible for shorter CBD times and kinetic energies below ~12 300 eV. This suggests that the layer structure is more complex than in the simple model sketched in Fig. 2, which will be discussed in the following.

For a first refinement step, we will now turn from the most bulk- to the most surface-sensitive measurements in our series. Figure 3 shows the Se 2p region measured at 2.1 keV excitation, resulting in an IMFP of λ = 1.5 nm. For all CdS/CIGSe samples, even for the 8.5 min CdS/CIGSe sample, a Se 2p signal is visible (but note the extremely high magnification factors given in Fig. 3, up to ×400 — such magnification factors are achievable thanks to the very high photon flux and count rates of the X-SPEC beamline). Using the model of a CdS overlayer of uniform thickness, an "effective" CdS thickness d can be derived from the Se 2p peak attenuation using $I = I_0 \cdot e^{-d/\lambda}$. The results are also included in Table I.

We find that the such-derived thickness values are generally smaller than the nominal ones, and, in particular, significantly smaller than the ones determined by the inelastic background analysis discussed above. In other words, the Se 2p intensity is higher than expected for the simple homogeneous CdS layer model. Several (real-world) sample imperfections could, in general, explain such behavior, in particular, pinholes, cracks, or scratches in the CdS layer, a diffusion (or segregation) of Se into the CdS layer, and/or readsorption onto the surface in the CBD bath. Here, pinholes, cracks, and scratches can be excluded since the peak intensities of *all* other absorber elements are attenuated as expected from the CBD-CdS film thickness; and this is shown here by an evaluation of the In 3d line intensity. As listed in Table I as well, the film thickness estimated from the attenuation of the In 3d line closely follows the thickness determined from the inelastic

TABLE I. CdS thicknesses of the CdS/CIGSe sample series, as determined from the inelastic background analysis for different photon excitation energies, as well as using the In 3d and Se 2p peak attenuation at 2.1 keV. The nominal thicknesses were estimated from scanning electron microscopy cross-sectional measurements of other samples with the same CBD times. All thicknesses are given in nanometers.

CBD time (min)	Nominal thickness estimate	From inelastic background analysis (keV)					From peak attenuation at 2.1 keV via $I = I_0 \cdot e^{-d/\lambda}$	
		14	12	9.0	6.3	2.1	In 3d	Se 2p
1.5	n.a.	2.2 ± 2.0	3.0 ± 1.5	4.5 ± 2.0	1.9 ± 0.5	4.0 ± 2.0	2.1 ± 0.5	1.3 ± 0.5
3.5	n.a.	14.8 ± 3.0	12.0 ± 4.0	15.5 ± 4.0	15.0 ± 4.0		15.6 ± 3.1	5.9 ± 1.5
5.0	18–20	26.5 ± 3.0	22.5 ± 4.0	25.5 ± 3.0	22.5 ± 5.0		>~20	7.4 ± 1.8
6.5	35	38.0 ± 4.0	33.0 ± 4.0	34.0 ± 3.0	37.0 ± 5.0			9.7 ± 2.2

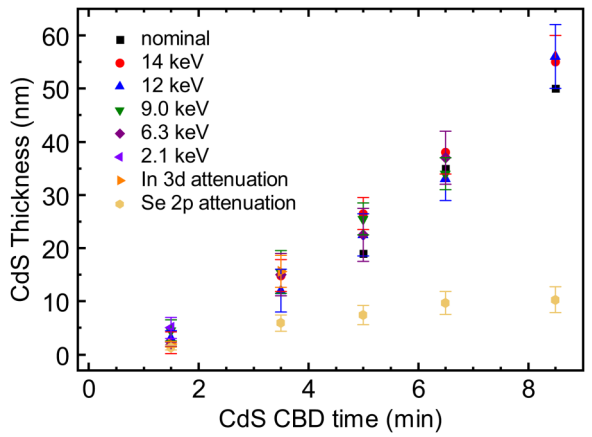

FIG. 5. CdS overlayer thickness, as determined from the background analysis, as well as In 3d and Se 2p peak attenuation as a function of CdS-CBD time. (Color online.)

background, and the In 3d signal is below the noise level for all samples with CBD times of 4 min or longer. Accordingly, the data suggest a diffusion/segregation of Se into or through the CdS layer. Based on a similar evaluation of XPS and XES data, such a diffusion of Se from $Cu(In,Ga)(S,Se)_2$ absorbers into CdS has been reported previously.[15,52,53] However, the XPS line intensities alone do not give any information on the actual diffusion profile or segregation model, i.e., very different depth distributions can result in the same line intensity behavior.[58] This "information gap" can be filled by using HAXPES and evaluating the inelastic scattering background related to the respective core-level peaks, as we will do in the following.

In the Se 2p region measured at 2.1 keV excitation (shown in Fig. 3), a clear trend in the background is visible as the CdS thickness increases. Relative to the intensity of the main line, the spectrum of the CIGSe absorber shows the largest steps in the background, which is related to the inelastically scattered Se 2p electrons from deeper inside the absorber. With increasing CBD time, the intensity of this background decreases relative to that of the Se 2p core level, and nearly no step in the background is visible for CBD times of 5.0 min and more. Apparently, the selenium atoms that give rise to the observed Se 2p core-level peak at 2.1 keV must be present at or close to the outermost surface, thus leading to no or only minimal inelastic scattering.

To quantify this, we have modeled the background of all 2.1 keV spectra. Note that the high magnification of the 6.5 and 8.5 min CdS/CIGSe spectra and the resulting lower signal-to-noise ratio does not allow for a very precise quantification. Nevertheless, the analysis indicates that Se is close to the surface. The background of the 5.0 min CdS/CIGSe sample can, in contrast, be modeled very well with a *thin Cd(S,Se) surface layer*, a pure CdS "intermediate" layer, and a small background signal from the Se-containing CIGSe absorber (as shown in the left panel of Fig. 4). We derive a thickness of 23 (±3) nm for the CdS layer. The analysis is not very sensitive to the exact thickness of the *Cd(S,Se) surface layer* but it is found to be less than ~2 nm. We note that the best description is found for a very small (but nonzero) Se concentration in this surface layer in the 1% range.

The background of the 3.5 min CdS/CIGSe sample in Fig. 3 is best described with a CdS thickness of 12 (±2) nm, a Se-containing surface layer within the upper ~2 nm, and a higher Se concentration (of 20–40%). However, as we will discuss in conjunction with Fig. 4, less surface-sensitive measurements (i.e., with higher excitation energies) of this sample suggest the need for an additional inhomogeneous CdS growth start model to properly describe the background (note that an inhomogeneous CBD-CdS growth start on CIGSe absorbers with and without Rb has indeed been reported earlier[48,59,60]).

Finally, the background of the 1.5 min CdS/CIGSe sample (at 2.1 keV) can be modeled with a ~5 nm Cd(S,Se) surface layer (concentration ~50%) and a CdS film thickness of 16 (±3) nm. Again, an "inhomogeneous-growth" model gives a significantly better description, which will be discussed below.

While Fig. 3 presented data at 2.1 keV for the different CdS layer thicknesses (and only near the Se 2p line), Fig. 4 now shows the wider Se 2s/2p region of the 8.5 (left) and 3.5 (right) min CdS/CIGSe samples, varying the excitation photon energy between 2.1 and 14 keV.

For the 8.5 min CdS/CIGSe sample, the Se 2s/2p main lines are barely visible for most excitation energies. For the 6.3 keV measurement, the inelastic background increases almost linearly, while it becomes more intense and structured at higher excitation energies. Most strikingly, the intensity at approximately 1550 and 1800 eV increases, which shows that, with increasing photon energy, more inelastically scattered electrons from the absorber are detected. To continue with the model of a Cd(S,Se) layer at the outermost surface, we have modeled the background of the 6.3, 9.0, 12, and 14 keV data with a 3 (±2) nm thin Cd(S,Se) surface layer, a CdS layer of 55 (± 5) nm, and an (infinitely thick) CIGSe absorber. For the 2.1 keV data, only a 1.5 (±1.0) nm thin Cd(S,Se) surface layer and no CIGSe absorber was used to model the background—in this case, as discussed above, no inelastically scattered Se electrons contribute to the background.

For the 9.0 keV data, we also find a weak Zn KLL Auger line (Zn 1s at ~9660 eV binding energy is excited by higher harmonics/orders of the undulator/monochromator) in the investigated energy window, which causes the background simulation algorithm to produce an "oscillating" background in that region. In the 2.1 keV data, a weak Zn 2p signal is found for all other CdS samples as well. Using the much stronger Cd 3d line, we derive a Zn/Cd ratio of approximately 0.003 (taking the respective IMFP, analyzer transmission function, and photoionization cross sections[61] into account). The source of such a minor Zn contamination is difficult to find; and most likely, it is a cross-contamination in one of the chemicals of the CdS-CBD step or the work area where Zn(O,S) depositions are also carried out. For the 6.3 keV data, we also find a rather strong Rb 2p signal (from the intentional RbF-PDT); and it causes a background artifact similar to that for the Zn line.

For the 3.5 min CdS/CIGSe sample (data shown as black lines in Fig. 4 right), the Se 2s and 2p signals are easily visible for all photon energies, indicating that the buffer layer is not yet very thick and/or Se is diffusing/segregating into/onto the CdS layer.

The 2.1 keV spectra show only a very small steps in the inelastic Se 2p background (compared to the Se 2p peak height), and, as discussed above, the data are best described by a very thin Cd(S,Se) layer with a Se concentration of ~1% at the surface and a 12 (± 2) nm thick CdS layer. In contrast, for higher excitation energies, the steps in the inelastic background are much more prominent. The latter suggests that the *majority* of selenium atoms is located in a buried region (rather than at the outermost surface). For a satisfactory description of the background, we, therefore, have to also take an inhomogeneity in CdS thickness into account, which was already mentioned in conjunction with Fig. 3. Note that we are studying real-world, polycrystalline thin-film samples, and, thus, a variation in the overlayer thickness across the surface is not at all surprising.

The inhomogeneous CdS growth start is modeled by a layer consisting of areas with two different thicknesses. Note that the QUASES software does not allow to simultaneously include two different layer thicknesses and the thin Cd(S,Se) surface layer. Thus, we omit the Cd(S,Se) surface layer to introduce the CdS thickness variations. Omitting the Cd(S,Se) surface layer is justifiable by the increased IMFP for higher excitation energies, leading to a lower relative contribution from a possible Cd(S,Se) surface layer.

The Se 2p and 2s background of the 9.0 keV data can best be described by combining two regions of thickness 4.8 nm (covering 23% of the overall area) and 18.6 nm (covering 77% of the area). For the 6.3 keV data, thicknesses of 4.6 (17% of the area) and 17.3 nm (83% of the area) give the best description. Both sets of parameters are within their respective margins of confidence, and slightly different parameter sets will also lead to a good description of the data. With this parameter set, the simulated background of the 3.5 min CdS/CIGSe sample in Fig. 4 is in much better agreement with the experiment than the simple overlayer model in Fig. 2.

To summarize the CdS overlayer thicknesses determined from the background analysis using the various models, Fig. 5 shows the CdS thickness as a function of CBD time. For 1.5 and 3.5 min, for which the inhomogeneous CdS buffer layer growth start plays an important role, the two discrete thicknesses derived from the model are averaged, weighted by the respective area contributions. The data are compared with the buffer layer thickness derived from the In 3d and Se 2p core-level attenuation in the 2.1 keV data using $d_{CdS} = -\lambda \cdot \ln(I/I_0)$ (see also Table I). While the thickness calculated from the In 3d attenuation fits with those determined from the inelastic background analysis, the values determined from the Se 2p strongly underestimate the film thickness. As discussed above, the latter is likely caused by the diffusion/segregation of Se into/through/onto the CdS buffer layer; and as a result, a simple interpretation of the Se 2p peak attenuation is not sufficient.

While no reliable nominal thicknesses are available for the 1.5 and 3.5 min CdS/CIGSe samples, the nominal thickness values (black squares) for the 5.0 min sample shows a slight underestimation of the background-determined thickness by ~3–5 nm. This can possibly be explained by the impact of the RbF-PDT, which enables a denser and faster growth of the CdS.[48] For the 6.5 and the 8.5 min CdS/CIGSe samples, the nominal thickness agrees, within the error bar, from that determined by the background models.

In addition to the Se signals, a Rb 2p signal is visible for all CdS/CIGSe samples, as shown in Fig. 6. It stems from the deliberate deposition of RbF onto the CIGSe absorber in the PDT step

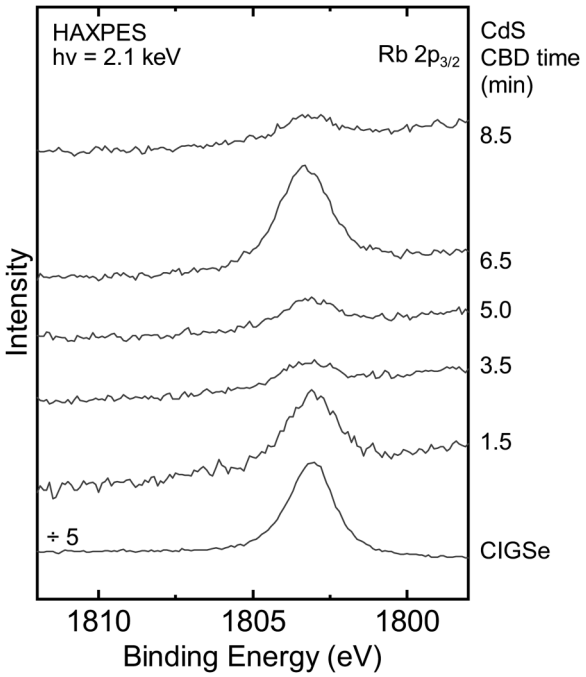

FIG. 6. Rb $2p_{3/2}$ peak for the CIGSe and CdS/CIGSe samples with increasing buffer layer CBD time, measured with an excitation energy of 2.1 keV.

and is not completely removed by the ammonia rinse prior to buffer deposition or during the CdS CBD itself.

The Rb 2p intensity is reduced by a factor of ~5 after the first CdS-CBD step. However, a clear signal remains visible for all samples, which varies strongly and unsystematically (e.g., for the 6.5 min sample). While no detailed analysis of the background is possible in this case due to the interfering Cd MNN Auger signal, the absence of an inelastic background step, together with the small λ of ~0.7 nm, suggests that Rb is present at the outermost surface of all samples. The quantitative amount of Rb (and hence the intensity in Fig. 6), thus, sensitively depends on the specific handling of each sample during and after CBD, especially when the wet surface is removed from the bath. Our results support our earlier findings of a diffusion/segregation of Rb into/onto the CdS layer.[13]

IV. SUMMARY AND CONCLUSIONS

A model study of CdS/Cu(In,Ga)Se_2 interfaces for thin-film solar cells was conducted using hard x-ray photoelectron spectroscopy from 2.1 up to 14 keV. The detailed structure of the CdS/CIGSe interface was determined by analyzing the core-level peaks and the background of inelastic scattered electrons at different photon energies. The surface-sensitive 2.1 keV measurements suggest that a less than ~ 2 nm thick Cd(S,Se) surface layer is present at the outermost CdS surface. The detailed background analysis of the Se 2p and 2s spectra at other excitation energies supports this finding. In this model, our analysis allows to

accurately determine the CdS film thickness (e.g., 55 ± 5 nm for the 8.5 min CdS/CIGSe sample). For the thinner CdS films, an inhomogeneous-growth start model gives insights into thickness variations at the early stages of the CdS deposition. The systematic use of different x-ray excitation energies combined with a mix of surface-sensitive *elastic* and bulk-sensitive *inelastic* signals enables a destruction-free, depth-varied picture of complex buried interfaces in applied material systems.

ACKNOWLEDGMENTS

Funding by the German Federal Ministry for Economic Affairs and Energy (BMWi) in project EFFCIS-II (Nos. 03EE1059A and 03EE1059E) is gratefully acknowledged. D. Hauschild, L. Weinhardt, and C. Heske thank the Deutsche Forschungsgemeinschaft (DFG) for funding in projects GZ:INST 121384/65-1 FUGG and GZ:INST 121384/66-1.

DATA AVAILABILITY

The data that support the findings of this study are available from the corresponding author upon reasonable request.

REFERENCES

[1]L. Weinhardt, D. Hauschild, and C. Heske, Adv. Mater. **31**, 1806660 (2019).
[2]D. Hauschild *et al.*, J. Phys. Chem. C **119**, 10412 (2015).
[3]S. Pookpanratana *et al.*, Appl. Phys. Lett. **93**, 172106 (2008).
[4]S. Kaya, D. Friebel, H. Ogasawara, T. Anniyev, and A. Nilsson, J. Electron Spectrosc. Relat. Phenom. **190**, 113 (2013).
[5]P. van der Heide, *Secondary Ion Mass Spectrometry: An Introduction to Principles and Practices*, 1st ed. (Wiley, New York, 2014).
[6]D. Hariskos, W. Hempel, R. Menner, and W. Witte, Appl. Sci. **10**, 1052 (2020).
[7]J. Han, C. Liao, L. Cha, T. Jiang, H. Xie, K. Zhao, and M.-P. Besland, J. Phys. Chem. Solids **75**, 1279 (2014).
[8]T. Adler, M. Botros, W. Witte, D. Hariskos, R. Menner, M. Powalla, and A. Klein, Phys. Status Solidi A **211**, 1972 (2014).
[9]T. Nelis and R. Payling, *Glow Discharge Optical Emission Spectroscopy: A Practical Guide, 2004* (Royal Society of Chemistry, Cambridge, 2003).
[10]D. Mercier, M. Bouttemy, J. Vigneron, P. Chapon, and A. Etcheberry, Appl. Surf. Sci. **347**, 799 (2015).
[11]V. R. Deline, W. Katz, C. A. Evans, and P. Williams, Appl. Phys. Lett. **33**, 832 (1978).
[12]A. Priebe, T. Xie, G. Bürki, L. Pethö, and J. Michler, J. Anal. At. Spectrom. **35**, 1156 (2020).
[13]D. Kreikemeyer-Lorenzo *et al.*, ACS Appl. Mater. Interfaces **10**, 37602 (2018).
[14]D. Hauschild *et al.*, Prog. Photovolt. **26**, 359 (2018).
[15]S. Pookpanratana, I. Repins, M. Bär, L. Weinhardt, Y. Zhang, R. Félix, M. Blum, W. Yang, and C. Heske, Appl. Phys. Lett. **97**, 074101 (2010).
[16]D. A. Duncan *et al.*, ACS Appl. Mater. Interfaces **7**, 16382 (2015).
[17]J. Stöhr, *NEXAFS Spectroscopy* (Springer-Verlag, Berlin, 1992).
[18]C. S. Fadley, R. J. Baird, W. Siekhaus, T. Novakov, and SÅL Bergström, J. Electron Spectrosc. Relat. Phenom. **4**, 93 (1974).
[19]S. Gusenleitner, D. Hauschild, T. Graber, D. Ehm, S. Tougaard, and F. Reinert, Surf. Sci. **616**, 161 (2013).
[20]C. S. Fadley, Surf. Sci. **19**, 231 (1993).
[21]S.-H. Yang, B. S. Mun, A. W. Kay, S.-K. Kim, J. B. Kortright, J. H. Underwood, Z. Hussain, and C. S. Fadley, J. Electron Spectrosc. Relat. Phenom. **114–116**, 1089 (2001).
[22]C. S. Fadley, J. Electron Spectrosc. Relat. Phenom. **178–179**, 2 (2010).
[23]S. Nemšák *et al.*, Nat. Commun. **5**, 5441 (2014).
[24]S. Tanuma, C. J. Powell, and D. R. Penn, Surf. Interface Anal. **21**, 165 (1994).
[25]H. Shinotsuka, S. Tanuma, C. J. Powell, and D. R. Penn, Surf. Interface Anal. **47**, 1132 (2015).
[26]S. Tougaard, see http://www.quases.com/home/ (last accessed July 12, 2021).
[27]A. X. Gray *et al.*, Nat. Mat. **10**, 759 (2011).
[28]C. S. Fadley, Nucl. Instrum. Methods Phys. Res. **547**, 24 (2005).
[29]C. Papp, G. Conti, B. Balke, S. Ueda, Y. Yamashita, H. Yoshikawa, Y. S. Uritsky, K. Kobayashi, and C. S. Fadley, J. Appl. Phys. **112**, 114501 (2012).
[30]S. Tougaard, Surf. Interface Anal. **26**, 249 (1998).
[31]S. Tougaard, J. Vac. Sci. Technol. A **39**, 011201 (2020).
[32]S. Tougaard, J. Electron Spectrosc. Relat. Phenom. **178–179**, 128 (2010).
[33]B. F. Spencer *et al.*, Appl. Surf. Sci. **541**, 148635 (2021).
[34]Y.-T. Cui *et al.*, J. Appl. Phys. **121**, 225307 (2017).
[35]S. Tougaard, J. Surf. Anal. **24**, 107 (2017).
[36]L. Meitner, Z. Phys. **9**, 131 (1922).
[37]P. Auger and C. R. Hebd, Séances Acad. Sci. **177**, 169 (1923).
[38]L. Meitner, Z. Phys. **17**, 54 (1923).
[39]D. Matsakis, A. Coster, B. Laster, and R. Sime, Phys. Today **72**, 10 (2019).
[40]H.-E. Mahnke, "Lise Meitner, β-decay and non-radiative electromagnetic transitions," Notes Rec. (published online 2020).
[41]P. Risterucci, O. Renault, C. Zborowski, D. Bertrand, A. Torres, J.-P. Rueff, D. Ceolin, G. Grenet, and S. Tougaard, Appl. Surf. Sci. **402**, 78 (2017).
[42]C. Zborowski and S. Tougaard, Surf. Interface Anal. **51**, 857 (2019).
[43]C. Zborowski, O. Renault, A. Torres, Y. Yamashita, G. Grenet, and S. Tougaard, Appl. Surf. Sci. **432**, 60 (2018).
[44]Best Research-Cell Efficiency Chart|Photovoltaic Research|NREL, see https://www.nrel.gov/pv/cell-efficiency.html (last accessed July, 12, 2021).
[45]M. Nakamura, K. Yamaguchi, Y. Kimoto, Y. Yasaki, T. Kato, and H. Sugimoto, IEEE J. Photovoltaics **9**, 1863 (2019).
[46]P. Jackson, R. Wuerz, D. Hariskos, E. Lotter, W. Witte, and M. Powalla, Phys. Status Solidi RRL **10**, 583 (2016).
[47]D. Hauschild, D. Kreikemeyer-Lorenzo, P. Jackson, T. M. Friedlmeier, D. Hariskos, F. Reinert, M. Powalla, C. Heske, and L. Weinhardt, ACS Energy Lett. **2**, 2383 (2017).
[48]T. M. Friedlmeier, P. Jackson, D. Kreikemeyer-Lorenzo, D. Hauschild, O. Kiowski, D. Hariskos, L. Weinhardt, C. Heske, and M. Powalla, in *Proceedings of the 2016 IEEE 43rd Photovoltaic Specialists Conference (PVSC)* Portland, OR, 5–10 June 2016 (IEEE, Piscataway, NJ 2016), pp. 0457–0461.
[49]S. Siebentritt *et al.*, Adv. Energy Mater. **10**, 1903752 (2020).
[50]N. Nicoara, R. Manaligod, P. Jackson, D. Hariskos, W. Witte, G. Sozzi, R. Menozzi, and S. Sadewasser, Nat. Commun. **10**, 3980 (2019).
[51]F. Pianezzi, P. Reinhard, A. Chirilă, B. Bissig, S. Nishiwaki, S. Buecheler, and A. N. Tiwari, Phys. Chem. Chem. Phys. **16**, 8843 (2014).
[52]C. Heske *et al.*, Appl. Phys. Lett. **74**, 1451 (1999).
[53]L. Weinhardt *et al.*, Appl. Phys. Lett. **96**, 182102 (2010).
[54]L. Weinhardt, R. Steininger, D. Kreikemeyer-Lorenzo, S. Mangold, D. Hauschild, D. Batchelor, T. Spangenberg, and C. Heske, J. Synchrotron. Rad. **28**, 609 (2021).
[55]P. Jackson, D. Hariskos, R. Wuerz, O. Kiowski, A. Bauer, T. M. Friedlmeier, and M. Powalla, Phys. Status Solidi RRL **9**, 28 (2015).
[56]S. Tougaard, Surf. Interface Anal. **25**, 137 (1997).
[57]M. Morkel, L. Weinhardt, B. Lohmüller, C. Heske, E. Umbach, W. Riedl, S. Zweigart, and F. Karg, Appl. Phys. Lett. **79**, 4482 (2001).
[58]S. Tougaard, J. Vac. Sci. Technol. A **14**, 1415 (1996).
[59]W. Witte, D. Abou-Ras, and D. Hariskos, Appl. Phys. Lett. **102**, 051607 (2013).
[60]W. Witte, D. Abou-Ras, and D. Hariskos, Phys. Status Solidi RRL **10**, 300 (2016).
[61]M. B. Trzhaskovskaya, V. I. Nefedov, and V. G. Yarzhemsky, At. Data Nucl. Data Tables **77**, 97 (2001).
[62]See the supplementary material at https://www.scitation.org/doi/suppl/10.1116/6.0001336 for HAXPES survey spectra at excitation photon energies of ~2.1, 6.3, 9.0, 12, and 14 keV.